Chaotically oscillating interfaces in a parametrically forced system

Miki U. Kobayashi*
Department of Applied Analysis and Complex Dynamical Systems, Graduate School of Informatics, Kyoto University, Kyoto 606-8501, Japan

Tsuyoshi Mizuguchi
Department of Mathematical Sciences, Osaka Prefecture University, Sakai 599-8531, Japan
(Received 19 July 2005; published 17 January 2006)

Structures and motions of a single interface exhibiting chaotic behavior are studied in the one-dimensional parametrically forced complex Ginzburg-Landau equation. There exist two kinds of chaotic interfaces whose differences are characterized by their chiral symmetry and the diffusivity of their motion. The transition between these behaviors is also investigated from the viewpoint of singularities of several dynamical variables, such as the diffusion constant, the resident time to each state, and the maximum trapping time to the unstable solution.

DOI: 10.1103/PhysRevE.73.016212 PACS number(s): 05.45.−a, 82.40.Bj, 89.75.Kd

I. INTRODUCTION

The structures and the motions of localized patterns, such as pulses and interfaces, are one of the main topics of dissipative nonlinear systems [1]. Especially the motions of interfaces play important roles in the behavior of bistable media [2–5]. The motion of a single interface is typically governed by the property of bulk region separated by the interface. In some systems with a kind of symmetry, however, a single interface moves by its internal structure [6]. We here focus on a one-dimensional complex Ginzburg-Landau equation with a parametric forcing term, in which various kinds of interfaces, e.g., a stationary solution, a steady moving solution, and various oscillating solutions, are reported [7–10].

In this paper, we report two kinds of chaotic motions of a single interface. The chaotically oscillating motions reported here show bistability due to the symmetry of the system, which is different from the previously reported ones in the experimental studies [11] and the numerical simulations [12]. The internal structures and the dynamical behavior of this system are characterized by a couple of order parameters which represent the symmetries and their breakdown. One of the chaotic interfaces shows clear diffusivity, and the diffusion constant is measured. Moreover, the transition between the two chaotic interfaces is investigated and singular behaviors of dynamical variables are numerically obtained which is partly predicted by theoretical considerations.

This paper is organized as follows: In Sec. II, we introduce the model equation and give a short review about single interfaces. In Sec. III, two kinds of chaotic interfaces are exhibited and the diffusivity of their motion is analyzed. Section IV is devoted to the analysis of the chaos-chaos transition from the viewpoint of singular behaviors of several dynamical quantities, such as the diffusion constant, the resident time to each state, and the maximum trapping time to the unstable solution. The summary is given in Sec. V.

*Electronic address: miki@acs.i.kyoto-u.ac.jp

II. MODEL

We consider a one-dimensional complex Ginzburg-Landau equation with a parametric forcing term:

$$\frac{\partial W}{\partial t} = (1+i\nu)W + (1+i\alpha)\frac{\partial^2 W}{\partial x^2} - (1+i\beta)|W|^2 W + \gamma\overline{W}, \tag{1}$$

where $W=X+iY$ is a complex variable. Parameters α, β, γ, and ν are real and γ is positive. $\bar{W}$ denotes the complex conjugate of W. The complex conjugate term of Eq. (1) represents an external forcing with approximately double the natural frequency with amplitude γ and $\beta-\nu$ stands for the frequency misfit. Equation (1) is bistable if the parameters hold the following conditions [7,8]:

$$\begin{cases} \gamma^2 > \dfrac{1+(\beta-2\nu)^2}{4} & \text{if } \beta(\beta-\nu) > \dfrac{1+\beta^2}{2}, \\ \gamma^2 > \dfrac{(\beta-\nu)^2}{1+\beta^2} & \text{otherwise,} \end{cases}$$

where there exists a pair of stable uniform states $\pm W_0$. In this region, Eq. (1) possesses kinklike solutions which connect W_0 and $-W_0$ in the one-dimensional system.

In the bistable case, several kinds of interfaces have been studied. Especially, the relation between the motion and the internal structure of a single interface is investigated as follows: For the variational case, i.e., $\nu=\alpha=\beta=0$, two types of interface known as Ising and Bloch wall are given in analytical forms. Ising wall is an odd function of $x-x_p$, where x is a space coordinate and x_p is the position of the interface, while Bloch wall contains an even component. Both types are stationary.

It is shown that Bloch wall moves with constant velocity in the weakly nonvariational case, $|\nu|, |\alpha|, |\beta| \ll 1$ [7]. The steady motion of the Bloch wall is coupled with the structural property characterized by the breakdown of so called *chiral symmetry*, the invariance under the transformation $W(2x_p-x,t) \to -W(x,t)$, where t is an arbitrary constant. For

the sake of generalization, we call the interfaces which keep the chiral symmetry *achiral* and the ones which break the chiral symmetry *chiral*, respectively.

In the case of the strongly nonvariational system, various oscillating behaviors of a single interface are observed [8,13]. The difference between oscillating interfaces and nonoscillating interfaces can be regarded as the breaking of *Galilei symmetry*, $W(x,t+\tau)=W(x-v\tau,t)$, where v is an averaged velocity of the interface. Both Ising and Bloch walls keep the Galilei symmetry for arbitrary τ, while the oscillating ones keep it only for discrete τ. From the viewpoint of chiral symmetry, the oscillating interfaces are also classified into two types, i.e., *achiral* and *chiral* [14]. Note that the chiral symmetry and its breakdown for this case should be considered in the sense of time average over its oscillating period. As is the nonoscillating case, the degree of breakdown of chiral symmetry is related to the mean drift velocity v, namely, $v=0$ for achiral and $v\neq 0$ for chiral.

III. CHAOTIC INTERFACES

Now, we focus on the chaotic version of achiral and chiral interface. A previous study shows that there is a chaotically oscillating interface in this model [13]. In order to investigate the bifurcation scenario and the chiral symmetry of the chaotic motion we perform numerical simulations of Eq. (1). We employ a particular set of parameters $\nu=1.6$, $\alpha=-0.5$, $\beta=1$ and vary γ as a control parameter in the bistable regime. The numerical method consists of a central finite difference method in space and the fourth-order Runge-Kutta in time. The time step is 0.001 and the space mesh is 0.1. To observe the behavior of a single interface the initial condition is chosen as a single kink: $W(x,0)=W_0$ if $x<L/2$ and $W(x,0)=-W_0$ if $x>L/2$ with additional fluctuations. Considering the symmetry of the system under the transformation $W\rightarrow -W$, the twisted periodic boundary condition with system size L, i.e., $W(0,t)=-W(L,t)$, is adopted for the sake of chasing the motion of a single interface with finite drift velocity.

To classify the interface from the viewpoint of the two symmetries, we introduce a couple of order parameters:

$$\chi_1(t) \equiv \int_0^L |X|(X_xY - Y_xX)dx,$$

$$\chi_2(t) \equiv \int_0^L |Y|(X_xY - Y_xX)dx. \tag{2}$$

By observing the behavior in the χ plane spanned by χ_1 and χ_2, several kinds of single interfaces are classified by their properties. First, χ_1 and χ_2 express the chiral symmetry because both of them vanish for Ising (steady achiral) solution, i.e., an odd function. In order to check the time averaged chiral symmetry, we adopt the distance between the origin $(\chi_1,\chi_2)=(0,0)$ and the center of mass of the orbit,

$$\chi_g \equiv \sqrt{\langle\chi_1\rangle^2 + \langle\chi_2\rangle^2}, \tag{3}$$

where $\langle\rangle$ denotes the average for long time enough for chaotic case. The internal structure of the interface is characterized by χ_g, i.e., it is regarded as *achiral* (*chiral*) if $\chi_g=0$ ($\chi_g\neq 0$), respectively [15]. Second, Galilei symmetry is exhibited in terms of the translational symmetry of the temporal behavior in the χ plane. Note that χ_1 and χ_2 are suitable for the twisted periodic boundary condition in the sense that they are invariant even if the interface passes through the boundary.

Figure 1 illustrates two typical spatiotemporal evolutions of the chaotic interfaces and the orbits in the χ plane. Figure 1(a) shows that the interface oscillates chaotically *with* mean drift velocity to a specific direction, while Fig. 1(b) shows the chaotically oscillating motion of the interface *without* mean drift. This difference is connected with the symmetry in the χ plane and the value of χ_g. The orbit of chiral case (C_-) is asymmetric about $(0,0)$ in the χ plane and $\chi_g\approx 0.1$ [Fig. 1(c)]. On the other hand, the orbit of achiral one (C_0) is symmetric and $\chi_g\approx 0$ [Fig. 1(d)]. We call these interfaces *chaotic chiral* and *chaotic achiral*, respectively.

To characterize the motions of these chaotic interfaces, let us concentrate on the diffusivity of the interfacial motion. The diffusive property of the chaotic motion is well characterized by the linearity of the variance of the position to the time [16,17]. Here, the variance $\sigma(t)$ of the interfacial position is measured to check the diffusivity. The definition of $\sigma(t)$ is

$$\sigma(t) \equiv \langle (x_p(t) - x_p(0) - \langle v\rangle t)^2\rangle, \tag{4}$$

where $x_p(t)$ is a position of the interface defined by the condition $\mathrm{Re}W(x_p,t)=0$. Note that $\pm L$ is added to the interfacial position when the interface moves across the boundary. v is a drift velocity of the interface.

For the chaotic achiral interface, we checked numerically that $\langle v\rangle\approx 0$. Therefore the variance, defined by Eq. (4), agrees with the mean-square displacement of the interfacial position $\langle[x_p(t)-x_p(0)]^2\rangle$. Figure 2 shows the mean-square displacement σ versus time for different values of γ. One finds that σ is approximately proportional to time t, which confirms the diffusive properties of chaotic achiral interfacial motion. The diffusion constants D for each value of γ can be estimated by the half value of the slope of corresponding lines in Fig. 2, which will be referred to in the next section.

For the chaotic chiral case, we also expect that σ increases linearly in proportion to the time, namely a diffusive motion *with* drift. The diffusion constant for the chiral case is, however, much smaller than that for the achiral case. Therefore the amplitude of short time scale oscillation cannot be ignored compared with $\sqrt{\sigma}$ during considerable computing time. For this reason, it is difficult to estimate the diffusion constant for chiral case systematically.

IV. SINGULARITIES

By increasing the control parameter γ, the chiral symmetry of chaotic interfaces changes without hysteresis from chiral to achiral at critical value γ_c. In this section, two singularities at this bifurcation point are studied in detail.

Figure 3 shows a bifurcation diagram. The Poincaré section in the χ plane [Fig. 3(a)] and χ_g for each γ [Fig. 3(b)]

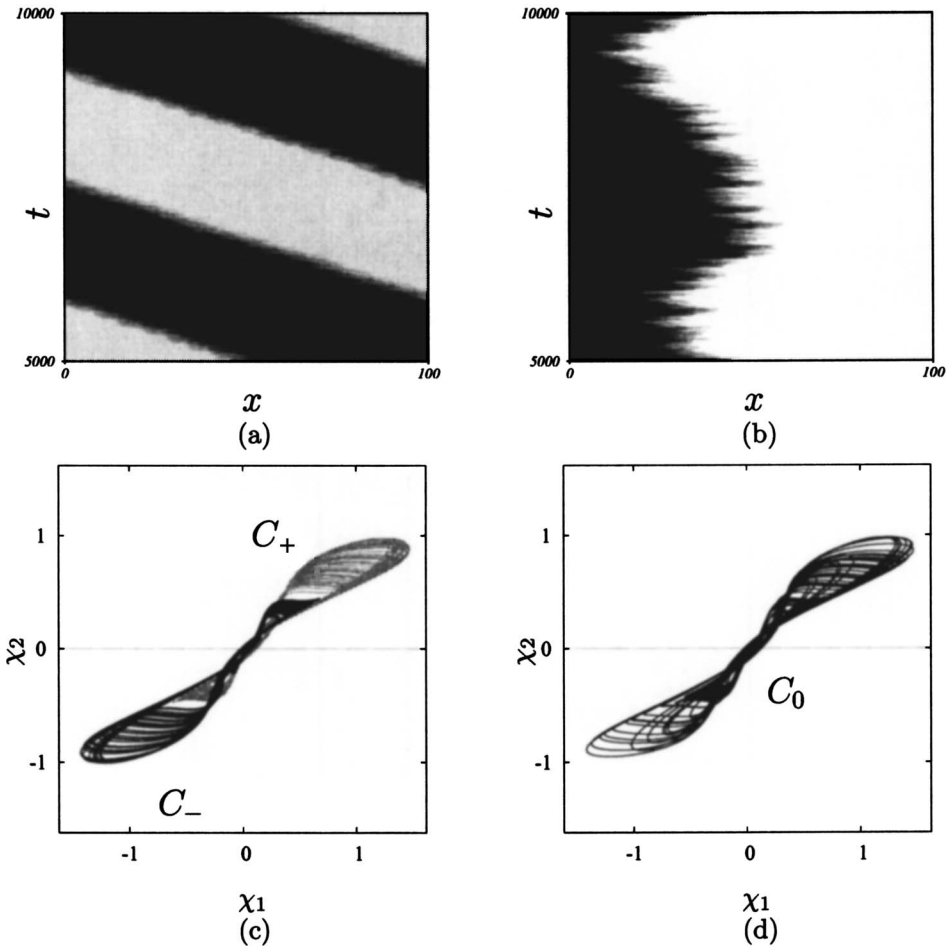

FIG. 1. Spatiotemporal patterns (a)(b) and the orbits in the χ plane (c)(d) of two kinds of chaotic interfaces, chiral interface ($\gamma=0.5945$) [(a) and (c)] and achiral one ($\gamma=0.5947$) [(b) and (d)]. The gray scale represents Re(W) from -1.26 (white) to 1.26 (black) in a spatiotemporal plot. The gray line denoted by C_+ corresponds to the orbit of chiral interfaces with positive mean drift velocity from a different initial condition.

are plotted. The chaotic motion arises at $\gamma_F \approx 0.594\,290\,8$ via a set of period-doubling bifurcations. At $\gamma_c \approx 0.594\,524\,8$, the attractor suddenly widens keeping chaotic behavior. Figure 3(b) shows that γ_c is the bifurcation point which separates the chiral regime ($\gamma < \gamma_c$) and the achiral regime ($\gamma > \gamma_c$). We now focus on the two types of singularities observed at the bifurcation point γ_c.

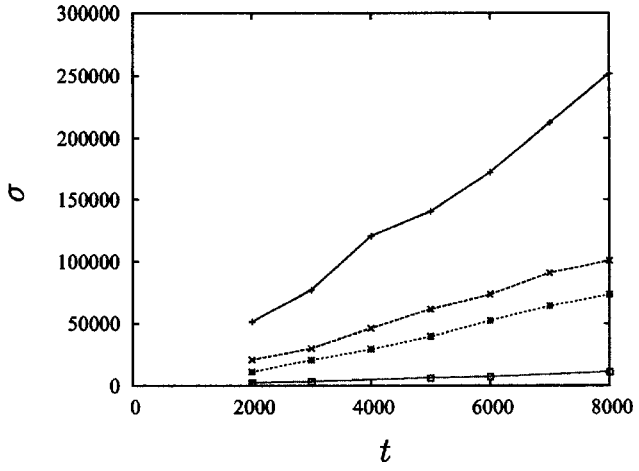

FIG. 2. Mean-square displacement of the interfacial position σ vs time t. Each line corresponds to different value of $(\gamma-\gamma_c)/\gamma_c$; 0.87×10^{-5}(+), 0.12×10^{-3}(×), 0.16×10^{-3}(*), and 0.24×10^{-2}(□).

A. Singularity from achiral side

First, we concentrate on a singularity near γ_c from the achiral side, i.e., $\gamma \to \gamma_{c+}$. Let us consider what happens in the χ plane at the bifurcation point γ_c. The motion of chaotic chiral interface involves a drift component as shown in Fig. 1(a). Note that the direction of the drift is either right or left depending on its initial condition. Thus in the χ plane there is a pair of strange attractors C_+ corresponding to the interface drifting to the right direction and C_- corresponding to the left direction for $\gamma < \gamma_c$. At $\gamma = \gamma_c$, both C_+ and C_- simultaneously touch the basin boundary B separating them and one strange attractor C_0 appears for $\gamma > \gamma_c$. This bifurcation is called attractor merging crisis (AMC) [18]. When $0 < \gamma - \gamma_c \ll 1$, the achiral attractor C_0 is constructed from fragments, so to speak, "wrecks" of C_+ and C_-. As a result, the state spends most of time on the wrecks of C_+ or C_- and sometime switches between them. Such the motion of $\chi(t)$ exhibits the diffusive motion of the interface which moves to only one direction for a long time and changes its direction then moves to the other direction and so forth. It is a kind of intermittency [19] and the intermittent motion is expected to be characterized by a resident time τ_R which is defined by an averaged time staying at one of the wrecks of the attractor. In this system, the internal degree of the solution is directly coupled with its instantaneous velocity of the interfacial position. We so defined τ_R as the average time when an interface keeps drifting in the same direction. We also measure

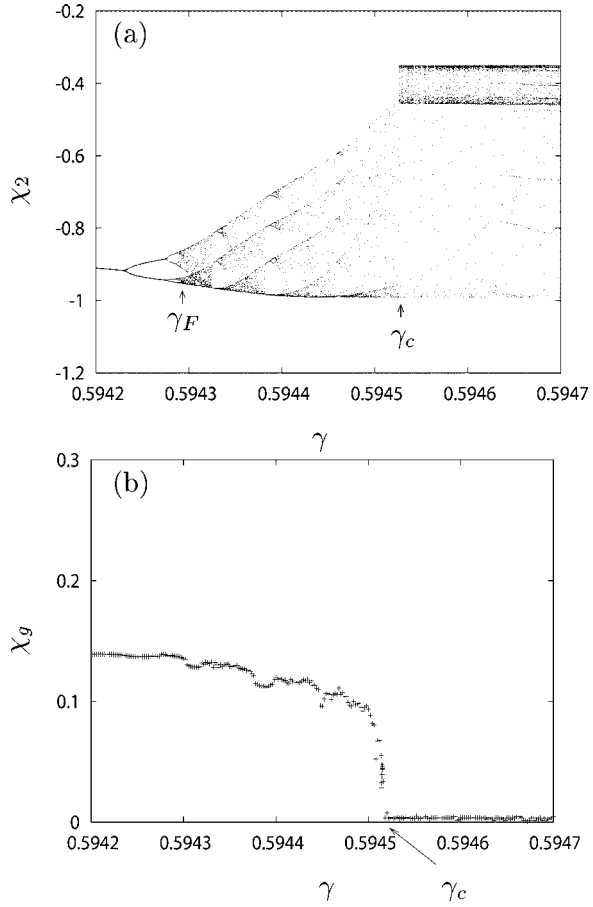

FIG. 3. (a) Bifurcation diagram concerning the periodicity. The horizontal axis shows γ and the vertical axis shows the value of χ_2 on appropriate Poincaré section in the χ plane. γ_F denotes the bifurcation point between chaotic and periodic motions. (b) Diagram for the chiral symmetry. The vertical axis represents χ_g. γ_c represents the bifurcation point between chiral and achiral behavior.

the diffusion constant $D(\gamma)$ because D is expected to be proportional to the correlation time of the interfacial velocity, which is plausible to be proportional to τ_R [16].

Figure 4 shows the numerical results. The diffusion constant D has a tendency to diverge at γ_c with a critical exponent $\alpha_1 \approx -0.48$ which is defined by $D \approx (\gamma - \gamma_c)^{\alpha_1}$. The divergent behavior of the resident time τ_R is well fitted with the same critical exponent α_1. The interpretation of the exponent α_1 remains open [18].

B. Singularity from chiral side

Next, let us consider the occurrence of a singularity when approaching it from the *chiral* side, i.e., $\gamma \to \gamma_{c-}$. Is it possible to foretaste the bifurcation phenomena when the system approaches to the critical point from asymmetric side?

Let us observe what happens near γ_c. Typical behavior of the interface near γ_c is depicted in Fig. 5. The solutions in both cases are chiral, and each of them has a finite drift velocity. There are, however, some temporal regions in which no drift motions are observed [indicated by double sided arrows in Fig. 5(b)] when γ approaches very close to γ_c. We expect that this driftless motion is a foretaste of the

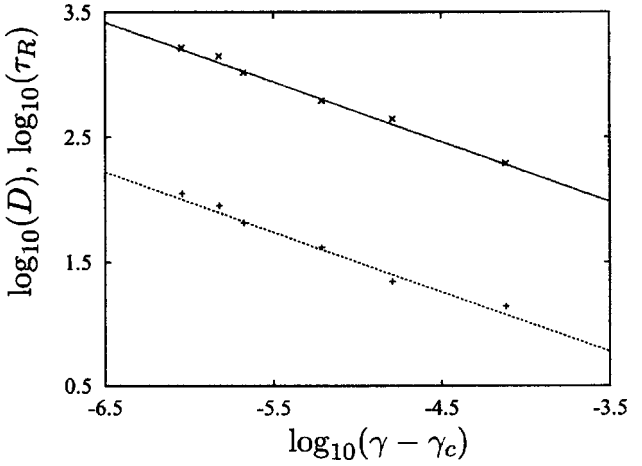

FIG. 4. Results of numerical simulations on logarithmic scale showing $D \approx (\gamma - \gamma_c)^{\alpha_1}$ (+) and $\tau_R \approx (\gamma - \gamma_c)^{\alpha_1}$ (×). The exponent α_1 and the critical value γ_c are fitted by D as $\alpha_1 = -0.48 \pm 0.3$ and $\gamma_c = 0.594\,523 \pm 6 \times 10^{-6}$, respectively.

bifurcation based on following consideration: For $\gamma < \gamma_c$ there exist two attractors, C_+ and C_-, and a basin boundary B which separates them. There is at least one saddle type solution S on B and the B coincides with the stable manifold of S. In the case of the system occurring AMC, as γ comes to γ_{c-} the outside orbit of C_+ or C_- approaches the basin boundary B, i.e., the stable manifold of S, and finally the orbit touches B at $\gamma = \gamma_c$. As a result, it is expected to be observed that the maximum trapping time τ_M near S becomes longer and longer as γ approaches γ_{c-} and finally it diverges [5,20].

We now estimate the function form of $\tau_M(\gamma)$. First, let the closest point on orbit C_+ to S be P and the distance between P and S be d. And let the point which is distant from S just by unity be Q (see Fig. 6). Here, we define the maximum trapping time τ_M as the time required to flow from P to Q. Second, let the maximum eigenvalue of the saddle solution S be λ, with an assumption that it is almost constant near γ_c. Next, we assume that the minimum distance d changes in the form $d \propto (\gamma_c - \gamma)^{\zeta}$, where we call ζ the asymptotic exponent. Using these definitions and assumptions, the maximum trapping time τ_M is given as

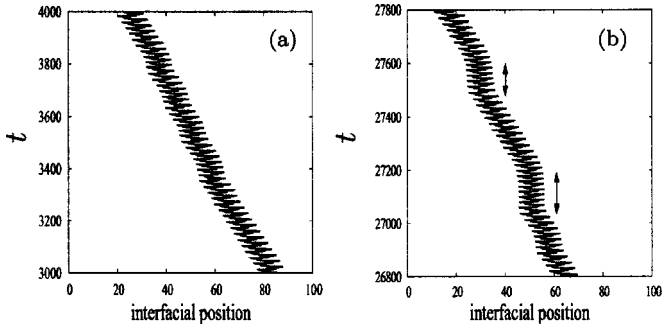

FIG. 5. Spatiotemporal patterns of the interfacial positions: (a) $(\gamma - \gamma_c)/\gamma_c = 2.49 \times 10^{-5}$ and (b) 3.02×10^{-6}. The horizontal axis shows the space coordinate, and the vertical axis shows the time. (b) Two arrows denote the time region in which the interface oscillates without drift motion.

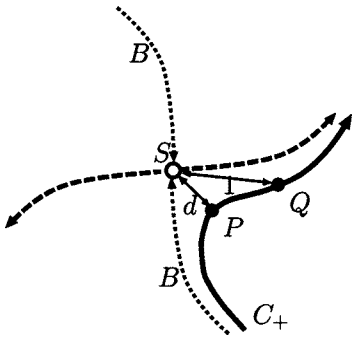

FIG. 6. Schematic diagram of the phase flow in the chiral regime near the bifurcation point. Open circle S represents the saddle solution. Dotted lines B are the basin boundary which coincides with the stable manifold of S. Dashed lines are the unstable manifold of S. Thick solid line denotes the typical behavior of closest orbit of the strange attractor C_+. Other part of orbit C_+ and the symmetric orbit C_- are not drawn for the simplicity. P is the closest point to S on the orbit C_+ and d is the distance between S and P. Point Q is distant from S just by unity. Note that S is considered to be a limit cycle actually.

$$\tau_M \propto -\frac{\zeta}{\lambda}\ln(\gamma_c-\gamma). \tag{5}$$

Unfortunately, we have not succeeded in obtaining an explicit form of the unstable solution S and it is difficult to measure each quantity in Eq. (5) directly. However, considering the fact that the dynamics of the system is well exhibited by the interfacial motion, the driftless motion is observed near S if S is an achiral periodic solution. Therefore we regard the maximum driftless motion time as τ_M and check its logarithmic behavior.

The actual measurement of $\tau_M(\gamma)$ is rather complicated: First, the position of interface $x_p(t)$ is defined by the condition $\mathrm{Re}W(x_p,t)=0$ as in the previous section. Second, we define the drift distance for each oscillation as the difference of the interfacial position of the successive timing, i.e., for an integer n, $\xi_n \equiv |x_p(t_n)-x_p(t_{n-1})|$, where t_n is the timing of the nth pass of Poincarè section and ξ_n is the drift distance of the nth oscillation. Next, the driftless motion time τ—which corresponds to the length of the double sided arrow in Fig. 5(b)—is defined as the time in which the drift distance per oscillation ξ_k is less than some threshold value ξ_*, i.e., $\tau \equiv t_n - t_m$ with the condition $\xi_k < \xi_*$ for $m<k<n$. Here, we set $\xi_*=1.0$ to distinguish the drifting motion and the driftless motion. Finally, we perform a long time simulation and measure τ_M as the maximum value of τ during the simulation for each γ.

Figure 7 indicates the logarithmic behavior observed in the numerical results, i.e., $\tau_M=\kappa\log_{10}(\gamma_c-\gamma)$ with fitting parameters $\kappa=-151\pm3$ and $\gamma_c=0.594\,524\pm3\times10^{-6}$, respectively. Note that these results are robust against the choice of technical quantities such as ξ_*, the definition of $x_p(t)$, and the Poincaré section.

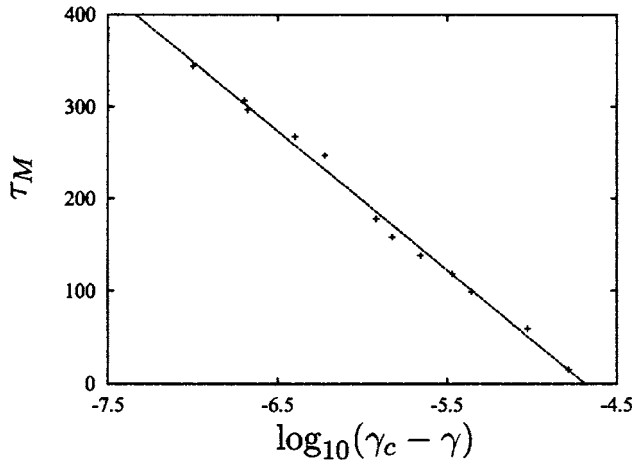

FIG. 7. $\gamma_c-\gamma$ vs τ_M with semilogarithmic plot. Symbols (+) denote the numerical results and the solid line is fitting line with $\tau_M=\kappa\log_{10}(\gamma_c-\gamma)$, where κ and γ_c are fitted.

V. CONCLUSION

We have established three important results: First, there are two types of chaotic interfaces, i.e., chiral and achiral. Second, in the parameter region used in this paper, the route to chaos is a period doubling bifurcation and the chaotic transition is an attractor merging crisis. Third, two singularities are investigated at the chaos-chaos transition point γ_c. One is the divergence of the diffusion constant D and the resident time τ_R in the achiral side with power law ($\alpha_1 \approx -0.48$). The interpretation of the value α_1 is a future problem. The other is the divergence of the maximum trapping time τ_M to the unstable solution S with logarithmic law in the chiral side. We think that κ is determined by the largest eigenvalue λ of S.

We conclude this paper by the discussion about the behavior of τ_M from the achiral side. Assume that the unstable solution S exists even in the achiral side. Then, τ_M is closely related to the invariant measure of achiral strange attractor C_0 near the stable manifold of S. If C_0 separates from S as $\gamma-\gamma_c$ increases, the singularity will be observed in the same way as in the chiral side. Or if S is embedded in C_0 in the achiral regime, no singular behavior of τ_M is expected. Further studies are required to answer to these questions.

ACKNOWLEDGMENTS

We acknowledge Professor H. Daido, Professor H. Fujisaka, Professor T. Chawanya, Professor E. Knobloch, K. Teramoto, and K. Ueda for valuable discussions. This work was partially supported by Grant-in-Aid for Scientific Research (C) No. 16605008 of the Ministry of Education, Culture, Sports, Science and Technology.

[1] Y. Kuramoto, *Chemical Oscillations, Waves and Turbulence* (Springer-Verlag, New York, 1984).
[2] K. Kawasaki and T. Ohta, Physica A **116**, 573 (1982).
[3] R. J. Deissler and H. R. Brand, Phys. Rev. Lett. **74**, 4847 (1995).
[4] T. Ohta, J. Kiyose, and M. Mimura, J. Phys. Soc. Jpn. **66**, 1551 (1997).
[5] Y. Nishiura, T. Teramoto, and K. Ueda, Chaos **13**, 962 (2003).
[6] A. Hagberg and E. Meron, Phys. Rev. Lett. **78**, 1166 (1997).
[7] P. Coullet, J. Lega, B. Houchmanzadeh, and J. Lajzerowicz, Phys. Rev. Lett. **65**, 1352 (1990).
[8] T. Mizuguchi and S. Sasa, Prog. Theor. Phys. **89**, 599 (1993).
[9] T. Kawagishi, T. Mizuguchi, and M. Sano, Phys. Rev. Lett. **75**, 3768 (1995).
[10] R. J. Deissler and H. R. Brand, Phys. Rev. Lett. **81**, 3856 (1998).
[11] L. Pastur, M. Henriot, and R. Ribotta, Phys. Rev. Lett. **86**, 228 (2001).
[12] R. J. Deissler and H. R. Brand, Phys. Rev. Lett. **72**, 478 (1994).
[13] T. Mizuguchi, Bussei Kenkyu **61**, 369 (1994).
[14] M. U. Kobayashi and T. Mizuguchi, Prog. Theor. Phys. Suppl. (to be published).
[15] In the numerical simulations, even for the analytically solved Ising solution, χ_g does not vanish because of numerical errors. Therefore we define a threshold value $\chi_g^*=10^{-3}$ and we adopt the condition whether $\chi_g > \chi_g^*$ or not as an actual criterion for the breakdown of the chiral symmetry. The threshold value 10^{-3} is chosen to distinguish Ising solution and the others numerically. The results of this paper are robust against the choice of χ_g^*.
[16] S. Grossmann and H. Fujisaka, Phys. Rev. A **26**, 1779 (1982).
[17] H. Koga, H. Fujisaka, and M. Inoue, Phys. Rev. A **28**, 2370 (1983).
[18] C. Grebogi, E. Ott, F. Romeiras, and J. A. Yorke, Phys. Rev. A **36**, 5365 (1987).
[19] E. L. Rempel and Abraham C.-L. Chian, Phys. Rev. E **71**, 016203 (2005).
[20] M. Argentina, P. Coullet, and L. Mahadevan, Phys. Rev. Lett. **79**, 2803 (1997).